

Raman scattering spectroscopy of liquid nitrogen molecules: An advanced undergraduate physics laboratory experiment

B. L. Sands,^{a)} M. J. Welsh, S. Kin, R. Marhatta, J. D. Hinkle, and S. B. Bayram^{b)}
Physics Department, Miami University, Oxford, Ohio 45056

(Received 23 June 2004; accepted 9 March 2007)

We describe a straightforward and highly visual experiment designed to demonstrate Raman scattering spectroscopy by measuring the vibrational energy spacing of nitrogen molecules in the liquid phase. Interpretation of the spectrum teaches the principles of elastic and inelastic light scattering and the intrinsic properties of molecules. The use of a pulsed Nd:YAG laser with high peak power leads to a plethora of nonlinear optical phenomena. The presence of highly visible stimulated Raman scattering greatly enhances the normal Raman-shifted signal, allowing for a more engaging laboratory experience in comparison to traditional Raman scattering experiments. © 2007 American Association of Physics Teachers.

[DOI: 10.1119/1.2721584]

I. INTRODUCTION

Raman scattering spectroscopy is a powerful technique for determining the internal structure of molecules and is an ideal demonstration for the study of vibrational transitions of gas and liquid phase molecules and crystals. The experiment described in this paper is designed for an advanced undergraduate spectroscopy laboratory and is intended to introduce students to Raman spectroscopy. The technique permits direct visual observation of nonlinear optical effects such as four-wave mixing (FWM),^{1,2} including coherent Stokes and anti-Stokes Raman scattering (CSRS and CARS, respectively),³ stimulated Raman scattering (SRS)⁴⁻⁶ and the associated cascaded multi-order SRS, and thermal blooming.⁷ In many of these experiments, the nonlinear effects occur simultaneously and easily when the incident laser power is above a certain threshold. Because these phenomena are unexpected, students are surprised when these effects suddenly appear during the course of a seemingly normal Raman scattering experiment. Additionally, the presence of stimulated Raman scattering greatly enhances the normal Raman-shifted signal, which allows for higher quality data. The experimental setup can be used as a traditional Raman scattering experiment and to explore many nonlinear optical effects by simply adjusting parameters of the laser.

Both linear and nonlinear Raman scattering spectroscopy have been used to help understand the physics of liquids by probing the effect of intermolecular forces on the structure and dynamics of pure liquids⁸ and solutions.⁹ The early development of nonlinear optics is reviewed by Bloembergen.¹⁰ Nonlinear CARS spectroscopy has been a very useful tool in combustion research,^{11,12} where the strong blackbody background makes spontaneous Raman signals more difficult to detect. Also, simultaneous temperature and species concentration measurements by CARS spectroscopy are important in time-resolved experiments probing combustion dynamics.¹³ More recent innovations of this technique have combined CARS spectroscopy with surface enhanced Raman spectroscopy (SERS) to detect signals with a resolution greater than the diffraction limit of the light.¹⁴⁻¹⁶ This form of CARS microscopy is currently being developed and has the potential to be very important in the study of nanostructures and biological chemistries beyond the limits imposed by other techniques. Stimulated Raman scattering and the associated cascaded multi-order SRS have been utilized

for generating coherent spectroscopic sources in a wide spectral range from the deep ultraviolet¹⁷ to the far infrared.¹⁸ These techniques have the advantage of opening up regions of the spectrum inaccessible by traditional coherent light sources.

The goals of this experiment center on three distinct levels of understanding: the existence of quantized vibrational energy states of the scattering molecules, the determination of the molecular bond strengths and the molecule's oscillation frequency from the Raman spectrum, and the ability to qualitatively describe features of the normal Raman spectrum and to observe and distinguish various nonlinear optical phenomena. Because students are likely to be unfamiliar with nonlinear optics, we let the students "discover" these phenomena by a careful analysis of the data. The striking visual nature of the experiment described here may pique the student's interest in spectroscopy and nonlinear optical phenomena and motivate students to investigate more detailed explorations in this area.

II. BACKGROUND

Students are well acquainted with resonant light absorption and emission from atoms and molecules. Scattering of light is different in that no permanent dipole moment is required. Light of any frequency will create an induced dipole oscillating with the light wave. Most often, such an induced oscillating dipole gives rise to re-radiation of light of equal energy. This process is known as elastic Rayleigh scattering. When light interacts with molecules, typically a small fraction of the light (about 1 in 10⁷ photons) is scattered inelastically by the normal Raman scattering process in which the energies of the incident and scattered photons are different. When the energy of the scattered photon is less than that of the incident photon, red-shifted light (Stokes Raman scattering) is generated. When the energy of the scattered photon is higher than the incident photon energy, blue-shifted light (anti-Stokes Raman scattering) is generated. The amount of energy exchanged between a molecule and photon is determined by changes in the vibrational and rotational quantum states of the molecule. This experiment uses liquid nitrogen as the scattering medium. In the liquid state, nearest-neighbor vibrational interactions will broaden the rotational

Raman spectrum so that individual lines overlap and cannot be resolved. Therefore, we only consider the vibrational Raman spectrum here.

Because the probability of inelastic scattering is very small in most media, Raman signals are notoriously difficult to observe. To compensate, a high power continuous-wave (cw) laser, such as an Ar-ion laser, can be focused on a sample to provide a high photon flux. Raman spectroscopy typically involves measuring the vibrational energy spacing ($v-v'=0-1$, where v and v' are vibrational quantum numbers denoting, respectively, the initial and final states following a transition) of the molecules.

In this paper we demonstrate the use of a pulsed Nd:YAG laser for measuring the Raman spectrum of liquid nitrogen. These lasers have been used in CARS and CSRS experiments^{19,20} and in liquid nitrogen²¹ and various gases^{22,23} for frequency conversion. Each pulse has a peak power 10^6 times that of cw lasers. Although high laser intensities may be undesirable for some research applications due to the potential of altering the physical properties of the sample, these high intensities provide much stronger Raman signals and a powerfully visual illustration of the nonlinear optical phenomena of interest here.

In this paper we present an experiment that starts as a traditional Raman scattering spectroscopy experiment and then stimulates students to explore and explain phenomena that cannot be explained by normal Raman scattering theory. For this reason, we now summarize the theory behind normal Raman scattering and then extend it to include nonlinear phenomena encountered in this experiment. We use this theory to interpret the experimental results. The phenomena studied in this experiment can be described straightforwardly using a semiclassical model.²⁴ The semiclassical model takes advantage of the wave-particle duality of light. The light-matter interaction can be described classically using a wave-mixing formalism, and the individual light-molecule interactions can be better visualized using energy level diagrams.

The fundamental physical mechanism underlying most of the phenomena discussed in this paper is normal Raman scattering.²⁵ The electric field of an incident pump laser beam linearly polarized along the z axis with frequency ω_p can be written as

$$\vec{E}(t) = E_p \hat{z} \cos(\omega_p t). \quad (1)$$

The light wave is assumed to be propagating along the x axis. This light induces an oscillating dipole in the molecule whose time-varying amplitude is given by

$$\vec{p}(t) = \alpha \vec{E}(t). \quad (2)$$

The polarizability α depends on the molecular species. In this experiment, we consider only homonuclear diatomics, such as N_2 , which are symmetric about all three principal axes. For nonsymmetric molecules, α becomes a second-rank tensor. Diatomic molecules are linear and possess only one vibrational degree of freedom. An expansion of α in terms of the normal coordinate q along the axis of vibration to first order gives

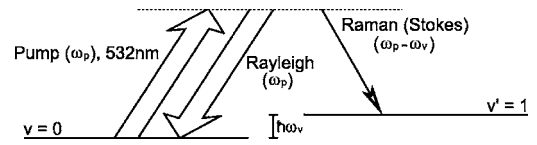


Fig. 1. Schematic of the normal Raman scattering process. The levels, labelled by vibrational quanta, indicate increasing potential energy. The frequencies of light involved are shown in parentheses with ω_v representing the molecular vibrational frequency. Molecules “pumped” by the second harmonic of the Nd:YAG laser at frequency ω_p to the virtual state (indicated by a dashed line) predominantly return to the ground state with no net energy change but occasionally return to an excited vibrational state, resulting in Raman scattered light.

$$\alpha(q(t)) = \alpha_0 + \left(\frac{\partial \alpha_0}{\partial q} \right) q(t). \quad (3)$$

If we assume the molecule vibrates sinusoidally with a frequency ω_v and use a trigonometric identity, we find that the expanded form of Eq. (2) simplifies to

$$\vec{p}(t) = E_p \hat{z} \left[\alpha_0 \cos(\omega_p t) + \frac{1}{2} \left(\frac{\partial \alpha_0}{\partial q} \right) q_0 (A + B) \right]. \quad (4)$$

In Eq. (4), the first term describes Rayleigh scattering and in the second term $A = \cos(\omega_p - \omega_v)$ represents Stokes Raman scattering and $B = \cos(\omega_p + \omega_v)$ represents anti-Stokes Raman scattering. The Raman scattering terms exist only if there is a change in the polarizability, which occurs with a changing vibrational state in the molecule. A generalization of this description to polyatomic molecules is treated in Ref. 25.

The normal Raman scattering process, which we described classically in the previous paragraph, can be described quantum mechanically by a photon annihilation/creation process. This process is analogous to the photon absorption/emission process. In terms of the energy level diagram of Fig. 1, the Raman scattered photons are absorbed to a virtual level of the molecule (photon annihilation), which subsequently emits a Stokes-shifted photon (photon creation) when a vibrational transition in the molecule changes its polarizability. Otherwise, photons are emitted with an unaltered frequency. The lifetime of the intermediate virtual level (or delay between photon annihilation and creation in the molecule) is exceedingly short ($\sim 10^{-14}$ s) and is comparable to the frequency of the vibrations in the molecule.

In addition to the Raman scattering process we have described, nonlinear optical processes such as four-wave mixing can be derived classically on the molecular scale by expanding $\vec{p}(t)$ to third order in $\vec{E}(t)$. Four-wave mixing can also be understood quantum mechanically as the annihilation of two photons and near simultaneous creation of two photons. In contrast, stimulated Raman scattering, another nonlinear process, cannot be described classically and is directly analogous to stimulated emission. An important point to be made with FWM is that, as with Rayleigh scattering, the light-molecule interactions take place with no change in the molecular energy state. Energy is then conserved in the mixing light fields. This energy conservation has important consequences that allow distinguishing four-wave mixing from normal and stimulated Raman scattering in our experiment. Maxwell’s wave equations, with the bulk polarization $\vec{P}(t, x)$ of the medium included, can be used to recognize this distinction.

In cgs units the nonlinear wave equation, under condition of no free charges or currents in the medium, takes the form

$$-\nabla^2 \vec{E}(t,x) = \frac{1}{c^2} \frac{\partial^2 \vec{E}(t,x)}{\partial t^2} + \frac{4\pi}{c^2} \frac{\partial^2 \vec{P}(t,x)}{\partial t^2}. \quad (5)$$

It is more convenient to represent $\vec{E}(t,x)$ and $\vec{P}(t,x)$ in the frequency domain. Under normal circumstances, $\vec{P}(\omega,x)$ is linearly proportional to the external electric field via the electric susceptibility χ . For intense fields, the bulk polarization includes higher order terms,

$$\vec{P}(\omega_4,x) = \vec{P}^{(1)}(\omega_4,x) + \vec{P}^{(2)}(\omega_4,x) + \vec{P}^{(3)}(\omega_4,x) + \dots, \quad (6)$$

where ω_4 denotes the frequency of the output wave. In isotropic media, $\vec{P}^{(2)}(\omega_4,x)$ is zero by symmetry. With the laser intensities used in this experiment, only the linear term and third-order nonlinear term,

$$\vec{P}^{(3)}(\omega_4,x) = \chi^{(3)} \vec{E}(\omega_1,x) \vec{E}(\omega_2,x) \vec{E}(\omega_3,x), \quad (7)$$

will be excited in our experiment. The \vec{E} fields in Eq. (7) represent separate mixing fields. The output frequency ω_4 will be some combination of the three mixing fields. The solution to Eq. (5) in the frequency domain, with the nonlinear polarization of Eq. (7), is of the form

$$\vec{E}(\omega_4,x) = A(\omega_4,x) e^{ik_4 x \hat{z}}, \quad (8)$$

where k_4 is the wave number of the light. This solution describes an output wave polarized along the z axis, which is taken to be the polarization direction of the pump laser. Substituting Eq. (8) into Eq. (5) and assuming that $A(\omega_4,x)$ does not change rapidly over the region of the nonlinear interaction (this slowly-varying amplitude approximation allows higher-order derivative terms to be neglected), the amplitude of the output wave resulting from a nonlinear interaction of the mixing fields is found to be²⁴

$$\frac{\partial A(\omega_4,x)}{\partial x} = \frac{ik_4}{2\epsilon(\omega_4)} \frac{4\pi P^{(3)}(\omega_4,x)}{e^{ik_4 x}}, \quad (9)$$

where $\epsilon(\omega_4)$ is the permittivity of the medium. Equation (9) can be used to derive the intensity of any wave involved in a FWM process. It is a fundamental result in nonlinear optics and is simplified for our purposes by assuming similarly polarized mixing fields provided from a single pump laser. Its derivation is accessible to advanced undergraduate students. Reference 24 fills in the details that have been omitted here for clarity. For a more thorough treatment of the physics, the students are referred to standard texts in nonlinear optics, such as Refs. 26–28.

If $P^{(3)}$ is expanded in Eq. (9), the phase factors from the four mixing waves can be combined to give $e^{i\Delta k x}$, where Δk is the sum of the wave vectors of the four mixing fields. The classical model can now be related to the quantum mechanical model we have discussed previously. Recall that four-wave mixing can be described quantum mechanically as the annihilation of two photons and subsequent creation of two photons. In the molecular system, annihilation of photons adds energy to the system (“positive” frequency) and photon creation releases energy from the system (“negative” frequency). Thus, in FWM processes $\Delta k = k_1 + k_2 - k_3 - k_4$. To

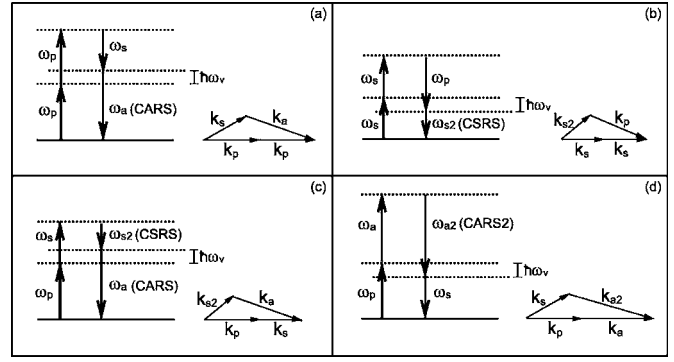


Fig. 2. Energy level diagrams for various four-wave mixing processes with virtual levels. Cases (a) and (b) represent typical coherent anti-Stokes (CARS) and Stokes (CSRS) Raman scattering processes, respectively. Cases (c) and (d) can exist for collinear pump and Raman-detuned beams. Both geometries are capable of producing CARS/CSRS spectra. The subscripts p , s , and a denote pump, Stokes, and anti-Stokes light, respectively, with numbers indicating the order of the Raman-shifted component with respect to ω_p . The molecular vibrational frequency is denoted as ω_v .

find the intensity of one of the created fields, Eq. (9) is integrated through an interaction length ℓ . If we assume the intensities of the mixing fields do not change significantly over the interaction length, we can express the intensity of light generated through a FWM process as

$$|A(\omega_4,x)|^2 = \frac{4\pi^2 \omega_4^2}{c^2 \epsilon^2(\omega_4)} \left[|\chi^{(3)}(\omega_1, \omega_2, -\omega_3)|^2 |A(\omega_1,x)|^2 \times |A(\omega_2,x)|^2 |A(\omega_3,x)|^2 \frac{\sin^2(\Delta k \ell / 2)}{(\Delta k / 2)^2} \right]. \quad (10)$$

Equation (10) is a maximum for $\Delta k = 0$. Because energy is conserved in the mixing light field, this result should be expected. This phase-matching condition was used in the experiment to distinguish between four-wave mixing processes and stimulated Raman scattering.

Figure 2 illustrates several different FWM processes. To resonantly excite this behavior, two coherent beams of frequency ω_p and $\omega_p \pm \omega_v$ are needed. Light generated from a FWM process with a frequency of $\omega_p + \omega_v$ [Fig. 2(a)] is known as coherent anti-Stokes Raman scattering (CARS) and light with a frequency of $\omega_p - 2\omega_v$ [Fig. 2(b)] is known as coherent Stokes Raman scattering. The probability of exciting one process over another is determined by the relative intensities of the two beams. Once these processes occur in the sample, other wave mixing scenarios are possible [Fig. 2(c) and Fig. 2(d)]. Higher order CARS and CSRS processes can also be generated with a sufficient pump laser intensity through the processes shown in Figs. 2(a) and 2(b). CARS and CSRS processes will produce rings with solid angles determined by the phase-matching conditions as illustrated in Fig. 2. In the experiment, the various optical processes can be distinguished by analyzing the spatial distribution of the output. Normal Raman scattering has a bipolar radiation field, reaching a peak intensity at 90° to both the direction of incident laser polarization and propagation. Stimulated Raman scattering produces laser-like, coherent beams that are

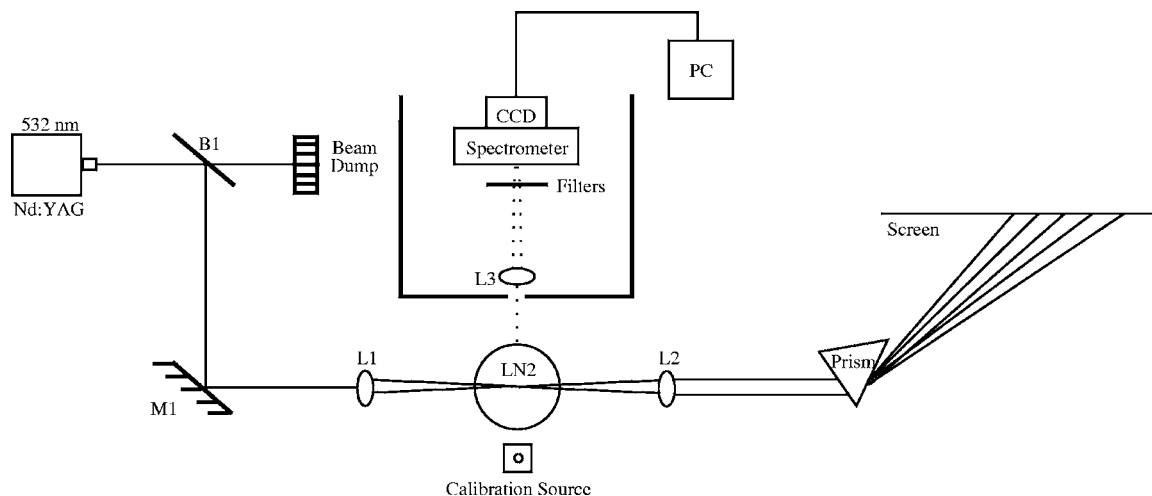


Fig. 3. A schematic diagram of the experimental apparatus. Roughly 7% of the incident laser power from the pulsed Nd:YAG laser was reflected off a beamsplitter B1. The laser beam was redirected via mirror M1 and focused into the center of the liquid nitrogen (LN2) dewar with a convex spherical lens L1. A second lens L2 was used to collimate the output beam. The Raman signal, indicated by a dashed line, was collected at right angles to the propagation direction of the laser by focusing light via a lens L3 onto the spectrometer entrance slit. A light tight box, indicated by the solid line, surrounded the detection scheme. A prism was used to disperse the output beam and better observe the nonlinear optical effects on a distant screen.

highly directional and centered within the CARS/CSRS rings. In the following section, we will demonstrate this distinction experimentally and describe other phenomena.

III. EXPERIMENT AND RESULTS

This experiment was carried out in liquid nitrogen. Aside from its easy and inexpensive availability, an important advantage of using liquid nitrogen as a Raman medium is that nitrogen exhibits large Raman gain⁵ which produces a higher amplitude signal. This fact, combined with a high intensity Nd:YAG laser, allows students to easily measure the Raman spectrum of nitrogen molecules.

The experimental setup is straightforward and is shown in Fig. 3. We used the second harmonic of a Nd:YAG pulsed laser at 532 nm, with a variable repetition rate up to 20 Hz. The pulse duration and the bandwidth of the laser were about 6 ns and 1 cm^{-1} , respectively. The laser beam was attenuated by reflecting $\sim 7\%$ of its power off a beam splitter B1. The remaining power was discarded in a beam dump for student safety and to avoid local boiling of the liquid nitrogen in the focal region. The incident laser, which had a beam diameter of 0.8 cm and approximate peak power of 1.4 MW, was directed toward the dewar by a mirror M1 and focused onto the sample using a 12.5 cm focal length convex spherical lens L1. An equal focal length lens L2 was placed on the opposite side of the dewar at a distance of twice the focal length from L1 to re-collimate the output beam. Students should move L2 slightly along the axis of the beam until the divergence of the beam beyond L2 is minimized. For additional safety, either the Nd:YAG beam should be greatly attenuated or a low power laser beam (for example, a HeNe laser) should be used to perform the initial alignment. An equilateral prism was alternatively used to disperse the collimated output beam to more easily observe the nonlinear optical effects on a distant screen. The normal Raman signal was collected by lens L3 at 90° to the propagation direction of the laser beam and focused onto the $25 \mu\text{m}$ entrance slit of a 0.25 m spectrometer with a 600 lines/mm (medium resolution) grating. The spectrometer was coupled to a 512×512 pixel,

thermoelectric-cooled charge coupled device (CCD) placed at the spectrometer's focal plane. The spectrometer's dispersion allowed observation of an approximately 60 nm band across the 512 pixel width of the CCD array, providing a limiting resolution of about 0.1 nm/pixel. The spectra recorded for this study were each from 1 s exposures of the CCD.

To minimize stray light entering the spectrometer and to isolate the Stokes and anti-Stokes bands, we used long- and short-pass filters, respectively, in front of the entrance slit depending on which spectral band was being measured. An additional aperture was also used to limit the collection lens L3 to accept light only from the focal region of the laser inside the dewar. This step was important for eliminating artificial signal broadening and ghost spectra from off-axis light entering the spectrometer. If done correctly, the Raman spectra should be single, sharp peaks. The long pass filter also served to prevent second-order diffraction of the Rayleigh and anti-Stokes bands from the spectrometer grating, which helped to correctly identify the Stokes bands. We also used a neutral density filter with $\sim 1\%$ transmission when measuring the very bright Rayleigh peak at 532 nm. In addition, the entire detection system was shielded with a black box wrapped with non-reflective flock paper. The box had a 1-cm-wide light entrance to reduce the ambient light.

The liquid nitrogen (LN2) container is an unsealed clear cylindrical pyrex dewar with a capacity of three liters and an interior pathlength of 8 cm. The evacuated lining between the inner and outer walls of the dewar minimizes interior boiling and reduces exterior condensation. Over time, the quality of this vacuum layer may degrade and these effects will be amplified. Interior bubbling causes rapid intensity fluctuations, but does not significantly effect the measured spectra. Fans can be used to further prevent condensation.

Before performing the experiment, the students were given a background in normal Raman spectroscopy similar to that given in the introduction. The students expected to see a laser-enhanced Raman signal with the spectrometer oriented 90° to the propagation direction of the laser beam. Because the liquid nitrogen is so cold, they also should

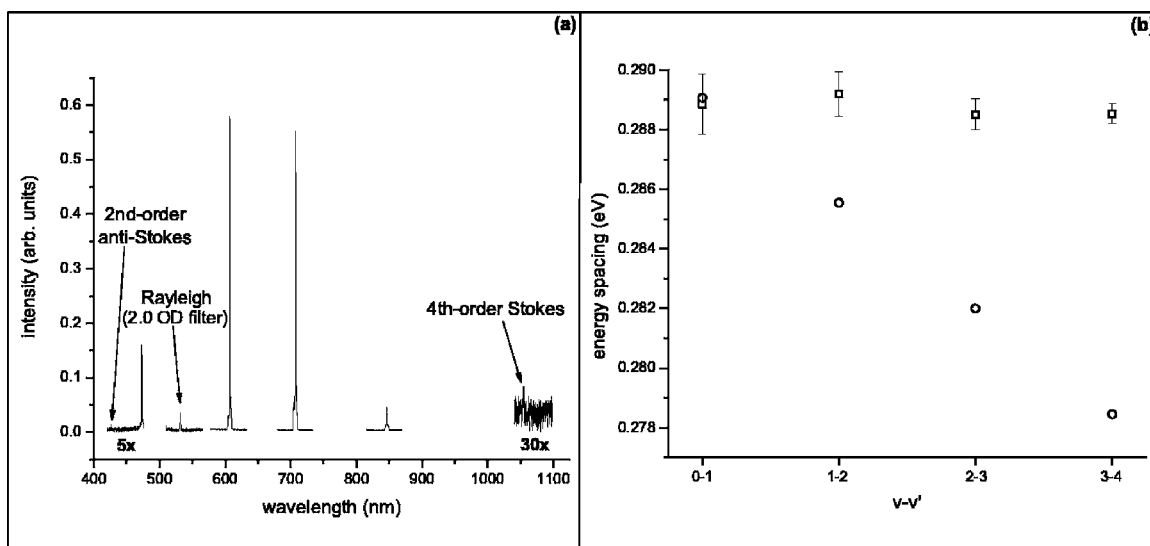


Fig. 4. (a) Raman scattering spectrum in liquid nitrogen. The Rayleigh scattered peak at 532 nm was greatly attenuated. The second-order anti-Stokes and fourth-order Stokes-shifted signals have been magnified for clarity. (b) Vibrational energy spacings as a function of $v-v'$. Our measured data (squares), derived from the spectra in (a) is displayed assuming the spectra correspond to the respective v' vibrational level. Reference energy spacings (circles) are shown for comparison (Ref. 29).

expect few vibrationally excited molecules and, therefore, anticipate a single Stokes-shifted peak. When discussing the data analysis, we try to convey the sense of discovery for the students as they are forced to explain their unexpected results and describe the steps they took to reach their conclusions.

A. Calibration

A medium resolution grating will generally not allow all the spectral features in this system to be measured simultaneously. For this reason, students separately measured each spectral feature. Such repetition also allowed the students to become familiar with calibration and data taking procedures. This section focuses on these procedures.

Before filling the dewar with liquid nitrogen, we recorded spectra around the wavelengths of interest with the laser light passing through the dewar to ensure that no fluorescence radiation from the various optical elements or scattered light from the dewar windows was being detected. The students used an argon capillary discharge tube placed behind the dewar along a line intersecting the spectrometer entrance slit and the focal region of the laser within the dewar to calibrate the spectrometer as shown in Fig. 3. After each calibration, another atomic capillary discharge source (any atomic source with known spectra in the region of interest is acceptable) was used to check the accuracy of the calibration. The wavelengths of the reference spectrum and the experimental Raman spectra were fit to a Lorentzian lineshape to determine the center wavelength. Comparison of the wavelength to the known wavelengths of the calibration sources showed a standard random error of ± 0.3 nm; this uncertainty was present in the measured vibrational Raman scattered spectra. If there are small deviations between the location of the focal region producing the Raman signal and the location of the calibration source, there may be a slight systematic error in the wavelengths. Such an error is easily detected if the measured Rayleigh scattering peak does not match the laser wavelength. Students should then check the alignment of the spec-

trometer, dewar, and calibration source, which should be in a straight line from the spectrometer entrance slit.

B. Measured results

Typical raw spectral data are shown in Fig. 4(a). Because the spectrometer was used with a medium resolution grating, the students took data for each of the spectral features shown in Fig. 4(a) separately. We combined the individual spectral images on a single wavelength scale for clarity. The intensity offsets for each spectral band were subtracted so that the spectra had a common baseline. Spectra of both anti-Stokes bands and the fourth-order Stokes band were magnified by the factors indicated in Fig. 4(a).

A wealth of information is available from these spectra. From the data students first determined the difference in energy between adjacent spectral bands. Students will likely recognize the spectra as normal Raman scattering from higher vibrational states. This interpretation may be plausible due to the high laser intensity, but turns out to be incorrect. To reach this conclusion, students should carefully analyze the spectra and compare it to available reference data. Our students compared their energy spacings derived from Fig. 4(a) to the known nitrogen vibrational energy spacings [see Fig. 4(b)]. [We determined the reference energy spacings in Fig. 4(b) using emission spectra from a well-known electronic quadrupole transition in nitrogen.²⁹] The energy spacings for our data (squares) are assumed to correspond to the vibrational levels indicated on the horizontal axis for which the known energy spacings are also displayed (circles). Because of the inverse relation between wavelength and energy, our constant random error of ± 0.3 nm results in error bars that decrease in magnitude for increasing v' . Because real molecules are not true harmonic oscillators, the vibrational energy spacing decreases for increasing v' . When students compared their data, there was a clear deviation from the reference data. The experimental energy spacings were the same for each Raman-shifted band. Students may recognize

this equality as the Raman spectra of the harmonic oscillator potential with equally spaced vibrational energy levels. The average value of the energy spacings was found to be 0.289 ± 0.001 eV (2330 ± 10 cm⁻¹), which matched the reference $v-v'=0-1$ vibrational energy spacing.²⁹ Knowing from the reference data that the nitrogen molecule cannot be represented by a harmonic oscillator, students should be skeptical of their results. Using different atomic sources to check individual calibrations and repeating the measurements if time permits helps to convince students that the deviations of their data from the reference data are real. To help illustrate these deviations the reference energy spacings can be used to predict where the spectral bands should have been detected. When this analysis is done for the $v-v'=3-4$ data point, for example, the deviation is nearly 20 nm from the predicted Raman-shifted wavelength.

To proceed with an explanation of these results, students may question, or be directed to question, why the output beam contains additional colors (orange is the most visible component if a doubled Nd:YAG laser is used as the pump). If additional colors are not obvious in the output beam, either the laser power may need to be increased or the focal lengths of the lenses outside the dewar shortened. If the colors were present and subsequently lost, condensation may have built up on the outside of the dewar. Figure 3 shows how to set up a prism to separate all the components and also demonstrate to students that the additional output beams are laser-like. With this information, students might recognize that the additional output beams correspond to the spectra that they previously measured. To convince themselves that the colors in the output beam are the same as the spectra they just acquired, students can optionally direct the (heavily attenuated) output into the spectrometer and record and compare the spectra. If there are multiple laser-like beams in the liquid nitrogen with wavelengths matching their measured spectra, students should ask if the spectra they measured really correspond to Raman scattering from higher vibrational levels. Rather than indicating Raman scattering from a perfect harmonic oscillator, the spectra are better explained as cascaded multi-order stimulated Raman scattering.²⁴ For very intense pump lasers, a Raman-shifted beam created by SRS off the $v-v'=0-1$ transition is intense enough to spawn another Raman-shifted beam and so on. This process yields both Stokes- and anti-Stokes-shifted beams that are of sufficient intensity to produce strong Rayleigh scattered signals, which were subsequently measured with the spectrometer, and accounts for the spectra in Fig. 4(a). We see that for our data in Fig. 4(b), the assumption that our measured Raman shifts corresponded to Raman scattering from higher vibrational levels was incorrect. The total observed number of output beams created in this manner depends on the conversion efficiency of the medium and the intensity of the pump laser beam. The lower detected intensities for the high-order Stokes components in Fig. 4(a) are due primarily to the downward sloping silicon detector efficiency. With the third harmonic of the Nd:YAG laser (354.6 nm) we were able to detect up to seven orders of this process because we were not limited by detector bandwidth. By using tunable dye lasers, this process has yielded over 50 Stokes and anti-Stokes orders that can be tuned to provide continuum coverage from the ultraviolet to the near infrared.³⁰ The lower detected intensities for the anti-Stokes components are a consequence of the liquid nitrogen. At the low temperature of 77 K, the

molecules overwhelmingly reside in the ground state. Because anti-Stokes bands result from scattering of molecules in an excited vibrational state, it is much less likely than Stokes scattering. The presence of a strong Stokes-shifted beam indicates a substantially elevated excited state population, thus allowing the anti-Stokes-shifted beams to “turn on.” This threshold behavior, characteristic of stimulated emission and stimulated scattering, can be nicely demonstrated by viewing the output through the prism. When gradually attenuating the input beam, the higher order components should “turn off” in order rather than gradually fading out.

Although the N₂ molecular potential is not harmonic, it is still a very good model, especially for nitrogen due to its deep potential well. In the simple harmonic approximation, knowledge of the vibrational energy yields information on the vibrational frequency of the molecule and the effective force constant of the molecular bond via the simple relation

$$\Delta E = \hbar \omega_v = \hbar \sqrt{\frac{\kappa}{\mu}}, \quad (11)$$

where κ is the effective force constant and μ is the reduced mass of the N₂ molecule (7 amu). For a vibrational energy of 0.289 eV derived from Fig. 4, $\omega_v = 4.39 \times 10^{14} \pm 2.0 \times 10^{12}$ rad/s, which corresponds to an effective force constant of 2250 ± 20 N/m. This value is in close agreement with the force constant of 2300 N/m in Ref. 31 for the N₂ molecule.

C. Visual observations

Now that students have learned that there is more occurring in this experiment than just Raman scattering, they can explore additional nonlinear phenomena. Visual observations of the nonlinear optical phenomena described in Sec. II are summarized in Fig. 5, which show two images of the output beam. FWM and SRS phenomena were observed by projecting the output beam from the dewar directly onto a screen [see Fig. 5(a)]. Figure 5(a) illustrates the differences between the nonlinear processes as described in Sec. II. The SRS is shown surrounded by FWM rings from both CARS and CSRS processes, which illustrate the phase-matching requirements implied from Eq. (10). The collinear SRS is overexposed and obscures much of the ring emission in the image, but a portion of it is visible. Sending the output beam through an equilateral prism [Fig. 5(b)] gives a better picture of the nonlinear processes occurring in the sample. Figure 5(b) visually shows the cascaded multi-order SRS discussed earlier: the first-order Stokes component shows strong SRS, with weaker SRS occurring in the second-order Stokes and first-order anti-Stokes components. Some four-wave mixing is also visible, surrounding the SRS beams in most of the spectral components. By varying the pump laser intensity, students can identify the thresholds for each of the stimulated Raman components and distinguish between SRS and FWM. Figure 5(b) illustrates this distinction with the second-order anti-Stokes component, which shows a FWM ring but no center stimulated component. Because the first order anti-Stokes beam is much less intense than its Stokes counterpart, it can generate a FWM ring at the second order anti-Stokes wavelength via the CARS process, but is not above the threshold intensity required to generate a stimulated component.

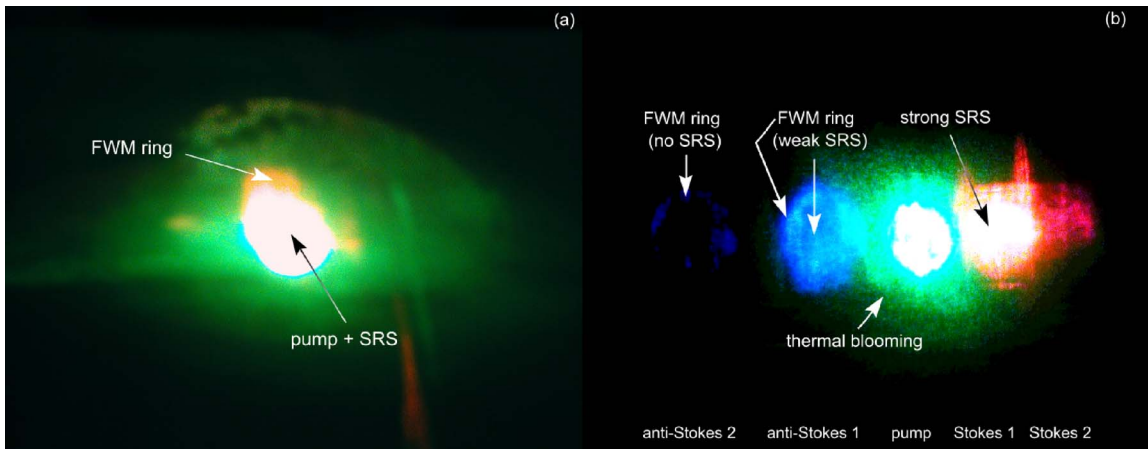


Fig. 5. (Color online) Images of typical output from our experiment. In (a) the output was imaged onto a screen outside of the dewar. The pump beam and stimulated Raman scattering beams run collinearly and form the center of the output. A portion of a four-wave mixing ring is also visible. Separating the output in a prism (b) helps to identify the various nonlinear phenomena. The labels on the spectra indicate multi-order SRS from the $\nu-\nu'=0-1$ vibrational transition.

One prediction students can make with respect to the discussion of the phase-matching conditions in Sec. II is that higher-order FWM is characterized by rings of increasing radius. In Fig. 5(b), the radius of the FWM rings appear to be the same because the first-order Stokes and anti-Stokes SRS beams are sufficiently intense to serve as separate pumps for FWM processes. As an example, the first-order anti-Stokes FWM ring is generated from the initial pump beam (at 532 nm) and the first-order Stokes beam [c.f., Fig. 2(a)], while the second-order anti-Stokes FWM ring is generated by the same process from the first-order anti-Stokes beam and the initial pump beam. The pump beams in both cases are separated by the same $\Delta\nu$, thus the relative phase-matching conditions will give the same divergence angle (neglecting the effects of dispersion). Students should be able to convince themselves of this fact by examining Fig. 2 and the phase-matching conditions derived from Eq. (10). The magnitude of the wavelength difference, and not the absolute wavelength, determines the radius of the FWM ring. If the output is sent through a spectrometer and imaged by a CCD camera, higher-order FWM rings of increasing radius may be visible.

Another factor that needs consideration when analyzing the visual output of this experiment is the nonlinear dependence of the dispersion with laser intensity within the liquid nitrogen. If the laser repetition rate can be changed, the students can see the effects of this nonlinear dependence by viewing the output (with or without prism) on a screen. We incrementally varied the repetition rate from 20 to 10 Hz and noticed that the radius of the output decreased as the repetition rate was decreased. This phenomenon, known as thermal blooming,⁷ occurs as the index of refraction is modified by rapid pulsing of the laser source. With each pulse, a significant vibrational excited state population is created in the interaction region. Because symmetric diatomic molecules such as N_2 cannot radiate, the excited state population is reduced by collisional quenching, converting vibrational energy to heat in the medium and changing the local refractive index. For sufficiently high repetition rates, this heat cannot diffuse out of the interaction region before the next pulse arrives, and the output laser beam becomes distorted. Below a repetition rate of about 13 Hz, the blooming became less

apparent because the added heat could sufficiently diffuse out of the interaction region between pulses. This result is consistent with other experiments performed in liquid nitrogen.²¹ Thermal blooming is important to consider if students make quantitative measurements of the FWM radii. The radii of the FWM rings are fixed by the phase-matching conditions. Thus, thermal blooming will inflate radius measurements. Operating at a low repetition rate will reduce this source of error.

IV. CONCLUSIONS

We have designed an advanced laboratory experiment to demonstrate high intensity Raman spectra and a multitude of nonlinear phenomena in liquid nitrogen via pulsed laser Raman scattering at 532 nm. In this experiment, the presence of strong stimulated Raman scattering in the liquid nitrogen generated multiple Raman-shifted orders off the $\nu-\nu'=0-1$ vibrational transition and greatly enhanced the normal Raman signal. This enhancement allows for an easier determination of intrinsic properties of the N_2 molecules such as the vibrational frequency and the force constant. The large signals measured were a huge advantage for achieving good quality spectra and accurate results. The presence of cascaded multi-order SRS in our sample mimicked a harmonic oscillator potential and proved to be a good lesson in careful data analysis for our students, who were not previously introduced to nonlinear optical phenomena. In such a case, students are first surprised by the contradictory results. However, explaining the contradictory results provided a very good transition to the field of nonlinear optics. The students could then explore the variety of nonlinear phenomena present in this experiment. We provided a brief introduction to the theory of nonlinear optics in order to make qualitative predictions that could be verified. Some instructive quantitative measurements, such as verifying energy conservation using the phase-matching conditions, are also possible with the experiment described here.

This experiment demonstrates some of the more common nonlinear optical phenomena, complementing an otherwise standard Raman scattering experiment. The spectacular visual nature of this experiment may motivate students to fur-

ther investigate the origin of these and other nonlinear effects not described here. With some modifications of the experiment, a large variety of additional phenomena can potentially be explored.²⁴ Although it has been shown that some effects do not occur in liquid N₂ or O₂,⁵ nonlinear optical phenomena can be observed in a variety of species without these limitations. Calcite and benzene are easy targets with high power lasers. Useful comparisons can also be made between different types of linear molecules if multiple Raman active samples are available, such as O₂ and CO₂. More complex polyatomic molecules may also be studied showing more diverse behavior than the simple linear diatomic molecule presented here.

Students can obtain an understanding of the light-matter interaction and the difference between linear and nonlinear scattering processes while measuring some fundamental properties of molecules. The presence of many additional effects, in contrast to a traditional Raman scattering experiment, was more exciting for the students, who were able to obtain a sense of discovery characteristic of real research experiences. This experiment may also be of interest to students studying biology, chemistry, and zoology.

ACKNOWLEDGMENTS

The authors wish to thank Professor Doug Marcum for his valuable suggestions. We gratefully acknowledge partial support from the National Science Foundation, Instrumentation and Laboratory Improvement Program Grant No. USE-9151932, Research Corporation (CC6119), and Miami University.

^{a)}Currently at U.S. Air Force Research Laboratory, Wright-Patterson Air Force Base, Ohio 45433.

^{b)}Electronic address: bayramsb@muohio.edu

¹P. D. Maker and R. W. Terhune, "Study of optical effects due to an induced polarization third order in the electric field strength," *Phys. Rev.* **137**, 801–818 (1965).

²R. Chiao and B. P. Stoicheff, "Angular dependence of maser-stimulated Raman radiation in calcite," *Phys. Rev. Lett.* **12**, 290–293 (1964).

³M. D. Levenson, "Coherent Raman spectroscopy," *Phys. Today* **30**(5) 44–49 (1977).

⁴N. Bloembergen, "The stimulated Raman effect," *Am. J. Phys.* **35**, 989–1023 (1967).

⁵J. B. Grun, A. K. McQuillan, and B. P. Stoicheff, "Intensity and gain measurements on the stimulated Raman emission in liquid O₂ and N₂," *Phys. Rev.* **180**, 61–68 (1969).

⁶G. Eckhardt, R. W. Hellwarth, F. J. McClung, S. E. Schwarz, D. Weiner, and E. J. Woodbury, "The stimulated Raman effect," *Phys. Rev. Lett.* **9**, 455–457 (1962).

⁷E. Wild and M. Maier, "Thermal blooming in liquid N₂ during high repetition rate stimulated Raman scattering," *J. Appl. Phys.* **51**, 3078–3080 (1980).

⁸M. J. Clouter, H. Kieffe, and R. K. Jain, "Pure vibrational Raman spectra of simple liquids: O₂, N₂, CO, CH₄, CF₄," *J. Chem. Phys.* **73**, 673–682 (1980).

⁹S. A. Akhmanov, F. N. Gadjiev, N. I. Koroteev, R. Y. Orlov, and I. L.

Shumay, "High-resolution cw CARS spectra of liquid nitrogen dissolved in liquefied Ar, Kr, O₂, CO, and CH₄," *Appl. Opt.* **19**, 859–862 (1980).

¹⁰N. Bloembergen, "Nonlinear optics and spectroscopy," *Rev. Mod. Phys.* **54**, 685–695 (1982).

¹¹P. Ewart and S. V. O'Leary, "Detection of OH in a flame by degenerate four-wave mixing," *Opt. Lett.* **11**, 279–281 (1986).

¹²A. C. Eckbreth, G. M. Dobbs, J. H. Stufflebeam, and P. A. Tellex, "CARS temperature and species measurements in augmented jet engine exhausts," *Appl. Opt.* **23**, 1328–1339 (1984).

¹³C. Brackmann, J. Bood, P.-E. Bengtsson, T. Seeger, M. Schenk, and A. Leipertz, "Simultaneous vibrational and pure rotational coherent anti-Stokes Raman spectroscopy for temperature and multispecies concentration measurements demonstrated in sooting flames," *Appl. Opt.* **41**, 564–572 (2002).

¹⁴N. Hayazawa, T. Ichimura, M. Hashimoto, Y. Inouye, and S. Kawata, "Amplification of coherent anti-Stokes Raman scattering by a metallic nanostructure for a high resolution vibration microscopy," *J. Appl. Phys.* **95**, 2676–2681 (2004).

¹⁵A. Volkmer, J.-X. Cheng, and X. Sunney Xie, "Vibrational imaging with high sensitivity via epidected coherent anti-Stokes Raman scattering microscopy," *Phys. Rev. Lett.* **87**, 023901-1–4 (2001).

¹⁶C. Heinrich, S. Bernet, and M. Ritsch-Marte, "Wide-field coherent anti-Stokes Raman scattering microscopy," *Appl. Phys. Lett.* **84**, 816–818 (2004).

¹⁷A. Goehlich, U. Czarnetzki, and H. F. Döbele, "Increased efficiency of vacuum ultraviolet generation by stimulated anti-Stokes Raman scattering with Stokes seeding," *Appl. Opt.* **37**, 8453–8459 (1998).

¹⁸P. Rabinowitz, B. N. Perry, and N. Levinos, "A continuously tunable sequential Stokes Raman laser," *IEEE J. Quantum Electron.* **22**, 797–802 (1986).

¹⁹J. B. Zheng, A. Leipertz, J. B. Snow, and R. K. Chang, "Simultaneous observation of rotational coherent Stokes Raman scattering and coherent anti-Stokes Raman scattering in air and nitrogen," *Opt. Lett.* **8**, 350–352 (1983).

²⁰A. C. Eckbreth and T. J. Anderson, "Simultaneous rotational coherent anti-Stokes Raman spectroscopy and coherent Stokes Raman spectroscopy with arbitrary pump-Stokes spectral separation," *Opt. Lett.* **11**, 496–498 (1986).

²¹S. R. J. Brueck and H. Kildal, "Efficient Raman frequency conversion in liquid nitrogen," *IEEE J. Quantum Electron.* **QE-18**, 310–312 (1982).

²²G. B. Jarvis, S. Mathew, and J. E. Kenny, "Evaluation of Nd:YAG-pumped Raman shifter as a broad-spectrum light source," *Appl. Opt.* **33**, 4938–4946 (1994).

²³A. D. Papayannis, G. N. Tsirikas, and A. A. Serafetinides, "Generation of UV and VIS laser light by stimulated Raman scattering in H₂, D₂, and H₂/He using a pulsed Nd:YAG laser at 355 nm," *Appl. Phys. B* **67**, 563–568 (1998).

²⁴G. S. He and S. H. Liu, *Physics of Nonlinear Optics* (World Scientific, Singapore, 1999).

²⁵G. Herzberg, *Molecular Spectra and Molecular Structure, I. Spectra of Diatomic Molecules* (Van Nostrand Reinhold, New York, 1950).

²⁶R. W. Boyd, *Nonlinear Optics* (Academic, San Diego, 1992).

²⁷G. C. Baldwin, *An Introduction to Nonlinear Optics* (Plenum, New York, 1969).

²⁸Y. R. Shen, *The Principles of Nonlinear Optics* (Wiley, New York, 1984).

²⁹A. Lofthus and P. H. Krupenie, "The spectrum of molecular nitrogen," *J. Phys. Chem. Ref. Data* **6**, 113–307 (1977).

³⁰T. Imasaka, T. Higashijima, S. Kawasaki, and N. Ishibashi, "Continuously tunable laser emission from the deep ultraviolet to the near infrared generated by a single optical system," *Appl. Opt.* **29**, 1727–1729 (1990).

³¹A. A. Radzig and B. M. Smirnov, *Reference Data on Atoms, Molecules and Ions* (Springer-Verlag, New York, 1985).